Dynamic analysis of externally excited NES-controlled systems via a mixed Multiple Scale/Harmonic Balance algorithm

Angelo Luongo, Daniele Zulli

Dynamic analysis of externally excited NES-controlled systems via a mixed Multiple Scale/Harmonic Balance algorithm

Angelo Luongo · Daniele Zulli

Abstract A general, nonlinear, multi-d.o.f. structure, excited by harmonic external force in 1:1 resonance with one of the modes of the system, is considered. The structure is attached to an essentially nonlinear oscillator, with small mass and damping (Nonlinear Energy Sink, NES). The scope of the NES is to passively control the amplitude of vibrations of the main structure. A mixed Multiple Scale/Harmonic Balance Method (MSHBM) is proposed to get the differential equations describing the slow- and fast-flow dynamics of the whole structure. The main advantage of the procedure is that no complexification-averaging is required, so that the analysis is reconducted in the framework of the classical perturbation techniques.

Keywords Multiple scale method · Harmonic balance · Nonlinear energy sink · Strongly modulated response

1 Introduction

Nonlinear Energy Sinks (NES) are mechanical devices, constituted by strongly nonlinear oscillators, attached to a main structure. Their mass is generally small, compared to that of the main system, and their goal is to absorb energy and to dissipate it, as a passive control device, through targeted energy transfers (TET) (see [1, 2] for an extensive background).

TET is a physical phenomenon that allows to convey energy associated with vibrations in a one-way, irreversible fashion, from a donor to a receptor. It was deeply investigated in the literature in the analytical, numerical, and experimental sense [3–7].

The main feature of the NES, consequence of its essential nonlinear nature, consists in the capacity of oscillate at any frequencies, giving rise of large band tuning with the structure to be controlled. The existence of relaxation oscillations and strongly modulated responses (SMR) is an other typical feature of this kind of systems (referred as *singular perturbation problems*), where both slow and fast dynamics are naturally involved (see [8, 9]).

Recently, these kind of devices have received great attention in the literature, being used in many applications. In [10, 11], a NES was applied to a main linear oscillator harmonically excited by a 1:1 resonant force. In [12, 13], multiple parallel NESs were considered to dissipate first-mode oscillations of a linear structure under impulse as well as harmonic forcing. In [14], nonsmooth NES was considered to control a two-d.o.f. system. In [15], NES was used to suppress aeroelastic instabilities on a rigid wing, modeled as a two-d.o.f. section-model, under stationary wind. In [16], a single NES is used to control oscillations of a long-span bridge prone to coupled flutter.

A. Luongo (✉) · D. Zulli
DISAT—University of L'Aquila, Via Giovanni Gronchi, 18, 67100 L'Aquila, AQ, Italy
e-mail: angelo.luongo@univaq.it

To analytically study the slow-flow dynamics of systems with NES, the researchers generally make use of two steps: (a) the complexification-averaging procedure by Manevitch [17], referred as CX-A, recently extended also to nonpolynomial nonlinearity [18] and piece-wise systems [14], and subsequently, (b) the Multiple Scale Method (MSM), [19]. In fact, due to the nonlinearizable nature of the equations of NES, it was stated in [20], where a grounded NES was studied, that "for this type of problem the standard analytical techniques from nonlinear dynamics (such as the method of multiple-scales, and the standard method of averaging), are not directly applicable, and an alternative approach must be followed"; accordingly, the complexification method was employed. Dealing with the same problem, three different methods were used in [21], namely, the method of harmonic balance, a combination of a shooting method and Floquet theory, and direct time integration, but not the MSM. In the same paper, the authors used an adapted version of the method of averaging, and defined their theoretical analysis as "limited." For all these reasons, it seems interesting to investigate the possibility of implementing a nonstandard version of the MSM, able to deal directly with general systems attached to essentially nonlinear oscillators.

In this paper, a general, nonlinear, multi-d.o.f. system under external resonant harmonic excitation is considered. A NES is attached to it, in order to control amplitude of vibrations. A mixed Multiple Scale/Harmonic Balance Method (MSHBM) is proposed, to get the critical manifold and the equations ruling both the slow-dynamics on it and the fast dynamics externally of it. The main advantage of the algorithm is that the initial complexification procedure is avoided, dealing directly with variables having clear physical meanings. An example, already analyzed in [2, 10, 11], is then considered, for which the asymptotic results are compared with numerical integrations. Effects on the solution of higher frequency components as well as analytical detection of SMR are addressed, also. However, a complete study of the dynamics, the influence of parameters modification, as well as the possible beneficial effect of the NES, are not fulfilled herein, being the aim of the paper turned to the presentation of the algorithm.

The paper is organized as follows. In Sect. 2, the algorithm is applied to a general system; in Sect. 3, a sample system is studied, in Sect. 4 results are discussed, and in Sect. 5 some conclusions are drawn.
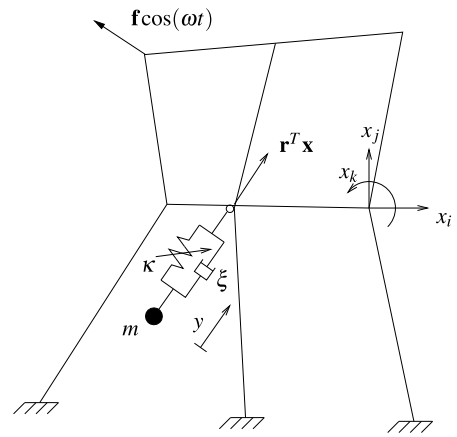

Fig. 1 Sketch of a multi-d.o.f. system equipped with a NES

2 The Multiple Scale/Harmonic Balance algorithm

A family of damped, nonlinear, multi-d.o.f. mechanical systems, under primary resonant harmonic excitation, is considered herein. The main system is equipped with an essentially nonlinear oscillator, behaving as a nonlinear energy sink (NES), attached at a point (see Fig. 1). The relevant nondimensional equations of motion of the whole system read:

$$\mathbf{M}\ddot{\mathbf{x}} + \mathbf{C}\dot{\mathbf{x}} + \mathbf{K}(\sigma)\mathbf{x} + \xi\left(\mathbf{r}^T\dot{\mathbf{x}} - \dot{y}\right)\mathbf{r}$$
$$+ \kappa\left(\mathbf{r}^T\mathbf{x} - y\right)^3\mathbf{r} + \mathbf{n}(\mathbf{x},\mathbf{x},\mathbf{x}) = \mathbf{f}\cos\omega t \quad (1)$$
$$m\ddot{y} - \xi\left(\mathbf{r}^T\dot{\mathbf{x}} - \dot{y}\right) - \kappa\left(\mathbf{r}^T\mathbf{x} - y\right)^3 = 0 \quad (2)$$

where: $\mathbf{x} = \mathbf{x}(t)$ is the time-depending N-dimensional column matrix of the displacements of the main structure; $\mathbf{M}$ is the mass matrix; $\mathbf{C}$ is the damping matrix, and $\mathbf{K}(\sigma)$ is the stiffness matrix, linearly depending on a structural parameter σ, $\mathbf{n}$ is the column of the (cubic) geometric nonlinearities, $\mathbf{f}$ is the column of the external force, modulated with frequency ω, $y = y(t)$ is the time-depending displacement of the added oscillator, m its mass, ξ its damping-ratio, and κ the coefficient of its essentially nonlinear (cubic) spring; $\mathbf{r}$ is the influence coefficient column; finally, the dot represents time-differentiation. It is assumed that when $\sigma = 0$, the external excitation is 1:1 resonant with one of the linear modes of the main structure (with NES disengaged), and no other resonance combinations are possible; therefore, σ acts as a detuning parameter. It is

convenient to introduce the relative displacement between main structure and NES, $z := \mathbf{r}^T\mathbf{x} - y$, so that Eqs. (1) and (2) become:

$$\mathbf{M}\ddot{\mathbf{x}} + \mathbf{C}\dot{\mathbf{x}} + \mathbf{K}(\sigma)\mathbf{x} + \xi\dot{z}\mathbf{r} + \kappa z^3\mathbf{r} + \mathbf{n}(\mathbf{x}, \mathbf{x}, \mathbf{x})$$
$$= \mathbf{f}\cos\omega t \qquad (3)$$
$$m(\mathbf{r}^T\ddot{\mathbf{x}} - \ddot{z}) - \xi\dot{z} - \kappa z^3 = 0 \qquad (4)$$

The dependent variables are rescaled through a nondimensional small parameter $\varepsilon > 0$, as $(\mathbf{x}, z) := \varepsilon^{1/2}(\tilde{\mathbf{x}}, \tilde{z})$, consistently with the presence of cubic nonlinearity. The damping is rescaled as $\mathbf{C} = \varepsilon\tilde{\mathbf{C}}$ and the external force as $\mathbf{f} = \varepsilon^{3/2}\tilde{\mathbf{f}}$, consistently with the idea to order both damping and excitation at the same level of the nonlinearity. The structural parameter σ is rescaled as $\sigma = \varepsilon\tilde{\sigma}$. The parameters of the NES are also rescaled, since both its mass and damping are assumed small: $(m, \xi) := \varepsilon(\tilde{m}, \tilde{\xi})$. The rescaling and series expansion of $\mathbf{K}(\sigma)$ lead to the following equations, after omission of tilde and division by $\varepsilon^{1/2}$:

$$\mathbf{M}\ddot{\mathbf{x}} + \varepsilon\mathbf{C}\dot{\mathbf{x}} + (\mathbf{K}_0 + \varepsilon\sigma\mathbf{K}_1)\mathbf{x} + \varepsilon\xi\dot{z}\mathbf{r}$$
$$+ \varepsilon\kappa z^3\mathbf{r} + \varepsilon\mathbf{n}(\mathbf{x}, \mathbf{x}, \mathbf{x}) = \varepsilon\mathbf{f}\cos\omega t \qquad (5)$$
$$\varepsilon m(\mathbf{r}^T\ddot{\mathbf{x}} - \ddot{z}) - \varepsilon\xi\dot{z} - \varepsilon\kappa z^3 = 0 \qquad (6)$$

where $\mathbf{K}_0 := \mathbf{K}(0)$ and $\mathbf{K}_1 := \partial\mathbf{K}(0)/\partial\sigma$.

According to the multiple scale method, independent time scales $t_0 := t$, $t_1 := \varepsilon t$, $t_2 := \varepsilon^2 t$, ... are introduced and, consistently, the derivatives expressed as $\frac{d}{dt} = d_0 + \varepsilon d_1 + \varepsilon^2 d_2 + \cdots$ and $\frac{d^2}{dt^2} = d_0^2 + 2\varepsilon d_0 d_1 + \varepsilon^2(d_1^2 + 2d_0 d_1) + \cdots$. Moreover, the dependent variables are expanded in series as

$$\begin{Bmatrix} \mathbf{x} \\ z \end{Bmatrix} = \begin{Bmatrix} \mathbf{x}_0 \\ z_0 \end{Bmatrix} + \varepsilon \begin{Bmatrix} \mathbf{x}_1 \\ z_1 \end{Bmatrix} + \varepsilon^2 \begin{Bmatrix} \mathbf{x}_2 \\ z_2 \end{Bmatrix} + \cdots \qquad (7)$$

Substituting in Eqs. (5) and (6) and collecting terms of the same order in ε, lead to the following perturbation equations:

order ε^0:

$$\mathbf{M}d_0^2\mathbf{x}_0 + \mathbf{K}_0\mathbf{x}_0 = 0 \qquad (8)$$

order ε^1:

$$\mathbf{M}d_0^2\mathbf{x}_1 + \mathbf{K}_0\mathbf{x}_1$$
$$= -2\mathbf{M}d_0 d_1\mathbf{x}_0 - \mathbf{C}d_0\mathbf{x}_0 - \sigma\mathbf{K}_1\mathbf{x}_0$$
$$- \xi d_0 z_0\mathbf{r} - \kappa z_0^3\mathbf{r} - \mathbf{n}(\mathbf{x}_0, \mathbf{x}_0, \mathbf{x}_0) + \mathbf{f}\cos\omega t_0 \qquad (9)$$

$$m(\mathbf{r}^T d_0^2\mathbf{x}_0 - d_0^2 z_0) - \xi d_0 z_0 - \kappa z_0^3 = 0 \qquad (10)$$

order ε^2:

$$\mathbf{M}d_0^2\mathbf{x}_2 + \mathbf{K}_0\mathbf{x}_2$$
$$= -\mathbf{M}(d_1^2\mathbf{x}_0 + 2d_0 d_2\mathbf{x}_0 + 2d_0 d_1\mathbf{x}_1)$$
$$- \mathbf{C}(d_2\mathbf{x}_0 + d_1\mathbf{x}_1) - \sigma\mathbf{K}_1\mathbf{x}_1 - \xi(d_0 z_1 + d_1 z_0)\mathbf{r}$$
$$- 3\kappa z_0^2 z_1\mathbf{r} - 3\mathbf{n}(\mathbf{x}_1, \mathbf{x}_0, \mathbf{x}_0) \qquad (11)$$
$$m(\mathbf{r}^T d_0^2\mathbf{x}_1 - d_0^2 z_1) - \xi d_0 z_1 - 3\kappa z_0^2 z_1$$
$$= 2m(d_0 d_1 z_0 - \mathbf{r}^T d_0 d_1\mathbf{x}_0) + \xi d_1 z_0 \qquad (12)$$

It should be noticed that, because of the vanishingly small values of the mass and damping, as well of the lack of linear stiffness, no equation of motion relevant to NES appears in the generator problem (order ε^0), which therefore describes the linear dynamics of the main structure alone (as if NES were disengaged).

The 1:1 external resonance with just one of the linear modes of the main system, together with the presence of damping, entails that the remaining nonresonant modes bring a higher-order contribution to the overall response. Therefore, only the contribution related to the resonant mode is retained in the solution of Eq. (8), i.e.,

$$\mathbf{x}_0(t_0, t_1, \ldots) = A(t_1, \ldots)\mathbf{u}e^{i\omega t_0} + cc \qquad (13)$$

where: $A(t_1, \ldots)$ is a complex modal amplitude, whose modulation on the slower time-scales must be evaluated; i is the imaginary unit; $i\omega$ and $\mathbf{u}$ are the resonant eigenvalue and (real) eigenvector of the problem $(\mathbf{K}_0 + \lambda^2\mathbf{M})\mathbf{u} = \mathbf{0}$, respectively; finally cc stands for complex conjugate.

The ε-order perturbation equations (9) and (10) are now addressed, and the NES equation (10) considered first. Since its (steady) solution cannot be expressed by elementary (nor Jacobi) functions, the harmonic balance method is used, letting

$$z_0(t_0, t_1, \ldots) = B_1(t_1, \ldots)e^{i\omega t_0} + cc \qquad (14)$$

where $B_1(t_1, \ldots)$ is a (first order) slowly modulated complex amplitude, to be evaluated. Other frequency components ($3\omega, 5\omega, \ldots$) are not considered here (see the next Sect. 4 for a discussion). Equations (13) and (14) are substituted in Eq. (10) and only ω-frequency terms are balanced. This step leads to

$$-m\omega^2(B_1 - rA) + i\xi\omega B_1 + 3\kappa B_1^2\bar{B}_1 = 0 \qquad (15)$$

where $r := \mathbf{r}^T\mathbf{u}$.

Equation (15) provides, at the first order of perturbation, an algebraic constrain between the (active) resonant amplitude of oscillation of the main structure and the (passive) amplitude of the NES elongation, B_1; it, therefore, describes a codimension-2 manifold in the state-space, on which the asymptotic dynamics take place. To get the (first order) real form of the manifold, the expressions $A(t) := \frac{1}{2}a(t)e^{i\alpha(t)}$ and $B_1(t) := \frac{1}{2}b(t)e^{i\beta(t)}$, are substituted in Eq. (15) and real and imaginary parts separated:

$$m\omega^2 r a \cos(\alpha - \beta) = m\omega^2 b - \frac{3}{4}\kappa b^3 \tag{16}$$

$$m\omega^2 r a \sin(\alpha - \beta) = -\xi \omega b \tag{17}$$

These latter, once squared and summed, provide

$$m^2\omega^4 r^2 a^2 = \left(m\omega^2 b - \frac{3}{4}\kappa b^3\right)^2 + \xi^2\omega^2 b^2 \tag{18}$$

which is a constrain between the two involved real amplitudes. Equation (15) (or (18)), however, is unable to describe motions which occur (in relaxation oscillation) externally to the manifold, which typically consist in very fast jumps. To capture this effect, a further perturbation equation must be tackled. Equation (9) is then considered, in which z_0 is assumed as in Eq. (14). By requiring that the resonant forcing term is orthogonal to the eigenvector $\mathbf{u}$ (solvability condition), the following condition is obtained:

$$d_1 A = (c_1 + i\sigma c_2)A + c_3 B_1 + i c_4 B_1^2 \bar{B}_1$$
$$+ i c_5 A_1^2 \bar{A}_1 + i c_6 f \tag{19}$$

where $f := \mathbf{u}^T \mathbf{f}$, and the expressions of the coefficients c_j are given in Appendix. By substituting Eq. (19) in Eq. (9) and by solving for $\mathbf{x}_1$, it holds

$$\mathbf{x}_1 = i A \mathbf{w}_1 e^{i\omega t_0} + \sigma A \mathbf{w}_2 e^{i\omega t_0} + B_1 \mathbf{w}_3 e^{i\omega t_0}$$
$$+ B_1^2 \bar{B}_1 \mathbf{w}_4 e^{i\omega t_0} + A^2 \bar{A} \mathbf{w}_5 e^{i\omega t_0} + \mathbf{w}_6 e^{i\omega t_0}$$
$$+ B_1^3 \mathbf{w}_7 e^{3i\omega t_0} + A^3 \mathbf{w}_8 e^{3i\omega t_0} + cc \tag{20}$$

where $\mathbf{w}_j$, $(j = 1, \ldots, 8)$ are defined in Appendix.

Equation (12) is finally considered: a new harmonic balance is carried out, assuming the following expression for z_1:

$$z_1(t_0, t_1, \ldots) = B_2(t_1, \ldots)e^{i\omega t_0} + cc \tag{21}$$

Substituting Eqs. (13), (14), and (20) in Eq. (12) and balancing the ω-frequency terms, the following equation is obtained:

$$-m\omega^2 B_2 + i\xi\omega B_2 + 3\kappa B_1^2 \bar{B}_2 + 6\kappa B_1 \bar{B}_1 B_2$$
$$+ (\xi + 2im\omega)d_1 B_1 - 2im\omega r d_1 A$$
$$+ m\omega^2 \big(i A w_1 + \sigma A w_2 + i B_1 w_3 + B_1^2 \bar{B}_1 w_4$$
$$+ A^2 \bar{A} w_5\big) + m\omega^2 w_6 = 0 \tag{22}$$

where $w_j := \mathbf{r}^T \mathbf{w}_j$, $j = 1, \ldots, 6$. Equations (15) and (22) can be reconstituted, using the definition $B := B_1 + \varepsilon B_2$, and coming back to the true time, to obtain:

$$(\xi + 2im\omega)\dot{B} - 2im\omega r \dot{A}$$
$$= \big(m\omega^2(1 - i w_3) - i\xi\omega\big)B$$
$$- \big(3\kappa + m\omega^2 w_4\big)B^2 \bar{B} - m\omega^2(r + i w_1 + \sigma w_2)A$$
$$- m\omega^2 w_5 A^2 \bar{A} - m\omega^2 w_6 \tag{23}$$

It appears that this equation now describes the dynamics of the amplitude B, differently from Eq. (15). The key-term containing $\dot{B}$ comes out only at the second-order, since it is affected by small coefficients ξ and m, thus revealing the nature of singular perturbation. In contrast, the term proportional to $\dot{A}$, which also appears at this order, does not add any qualitative new contributions, being ruled by Eq. (19).

If the perturbation procedure is truncated at order ε for the main system equation, the solvability condition (19) can be written in terms of the true time:

$$\dot{A} = (c_1 + i\sigma c_2)A + c_3 B + i c_4 B^2 \bar{B} + i c_5 A^2 \bar{A} + i c_6 f \tag{24}$$

To get the polar form of Eqs. (24) and (23), $A(t) := \frac{1}{2}a(t)e^{i\alpha(t)}$ and $B(t) := \frac{1}{2}b(t)e^{i\beta(t)}$ are substituted in them and real and imaginary parts separated, thus obtaining (from Eq. (24)):

$$\dot{a} = c_1 a + c_3 b \cos(\alpha - \beta) + \frac{c_4}{4}b^3 \sin(\alpha - \beta) \tag{25}$$

$$a\dot{\alpha} = \sigma c_2 a + c_3 b \sin(\alpha - \beta) + \frac{c_4}{4}b^3 \cos(\alpha - \beta)$$
$$+ \frac{c_5}{4}a^3 + c_6 f \tag{26}$$

and (from Eq. (23))

$$\xi\dot{b} - 2\omega m b\dot{\beta} + 2\omega m r\left(\dot{a}\sin(\alpha - \beta) + a\dot{\alpha}\cos(\alpha - \beta)\right)$$

$$= m\omega^2 w_1 a\sin(\alpha - \beta)$$

$$- m\omega^2(r + \sigma w_2)a\cos(\alpha - \beta) + m\omega^2 b$$

$$- \left(m\omega^2 w_4 + 3\kappa\right)\frac{b^3}{4} - m\omega^2 w_5\frac{a^3}{4}\cos(\alpha - \beta)$$

$$- m\omega^2 w_6\cos\beta \tag{27}$$

$$2\omega m\dot{b} + \xi b\dot{\beta} - 2\omega m r\left(\dot{a}\cos(\alpha - \beta) - a\dot{\alpha}\sin(\alpha - \beta)\right)$$

$$= -m\omega^2 w_1 a\cos(\alpha - \beta)$$

$$- m\omega^2(r + \sigma w_2)a\sin(\alpha - \beta)$$

$$- \left(m\omega^2 w_3 + \omega\xi\right)b - m\omega^2 w_5\frac{a^3}{4}\sin(\alpha - \beta)$$

$$+ m\omega^2 w_6\sin\beta \tag{28}$$

The nonlinear singular perturbation problem Eqs. (25)–(28) describes the dynamics of the main system attached to the NES, in terms of the real dependent variables a, b, α, β. Its equilibrium points, determined taking $\dot{a} = \dot{b} = \dot{\alpha} = \dot{\beta} = 0$, represent periodic oscillations in the displacement x, z.

3 Sample systems and numerical results

A sample system, already studied in [2, 11], is considered here to check the reliability of the method presented in Sect. 2. A complete study of the dynamics of the proposed example, as well as of the possible beneficial effect of the NES, however, are not fulfilled herein, since they are out of the aim of this paper.

The main system consists of a 1-d.o.f. linear undamped system, with attached NES, a sketch of which is shown in Fig. 2. The nondimensional equations of motion are:

$$\ddot{x} + \left(\omega^2 + \sigma\right)x - \xi(\dot{y} - \dot{x}) - \kappa(y - x)^3 = f\cos\omega t \tag{29}$$

$$m\ddot{y} + \xi(\dot{y} - \dot{x}) + \kappa(y - x)^3 = 0 \tag{30}$$

that, for $z := x - y$, become:

$$\ddot{x} + \left(\omega^2 + \sigma\right)x - \xi\dot{z} - \kappa z^3 = f\cos\omega t \tag{31}$$

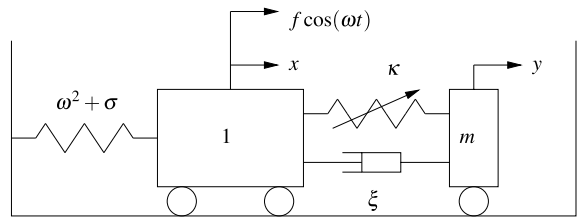$$m(\ddot{z} - \dot{x}) + \xi\dot{z} + \kappa z^3 = 0 \tag{32}$$
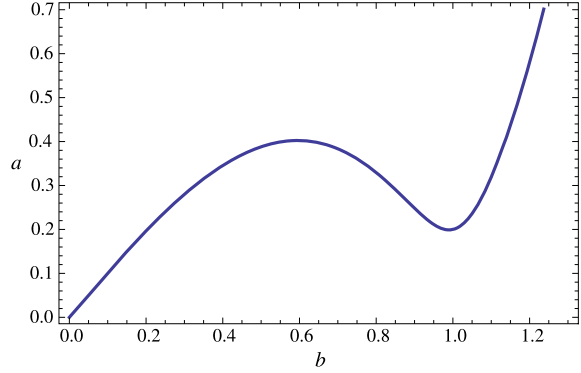

Fig. 2 Sketch of a analyzed system

Fig. 3 Nonlinear manifold when $m = 0.05$, $\xi = 0.01$, $\kappa = 0.067$, $\omega = 1$

Therefore, comparing it with Eqs. (3) and (4), it results:

$$N = 1, \qquad \mathbf{x} = x, \qquad \mathbf{M} = 1, \qquad \mathbf{C} = 0,$$

$$\mathbf{K}_0 = \omega^2, \qquad \mathbf{K}_1 = 1, \qquad \mathbf{n}(\mathbf{x}, \mathbf{x}, \mathbf{x}) = 0, \tag{33}$$

$$\mathbf{f} = f$$

The nonlinear manifold, Eq. (18), becomes

$$\left(\frac{3\kappa b^2}{8m\omega} + \frac{\omega b}{2}\right)^2 + \left(\frac{\xi b}{2m}\right)^2 - \frac{\omega^2 a^2}{4} = 0 \tag{34}$$

and it is shown in Fig. 3 for $m = 0.05$, $\xi = 0.01$, $\kappa = 0.067$, $\omega = 1$ (which is the set of numerical values considered in [2, 11]).

The (first order) solvability condition reads:

$$\dot{A} = \frac{i\sigma}{2\omega}A - \frac{\xi}{2}B - \frac{3i\kappa}{2\omega}B^2\bar{B} - \frac{if}{4\omega} \tag{35}$$

and the (second order) harmonic balance becomes:

$$2im\omega\dot{A} - (2im\omega + \xi)\dot{B}$$

$$= m\omega^2 A + \left(i\xi\omega - m\omega^2\right)B + 3\kappa B^2\bar{B} \tag{36}$$

In polar form, they assume the forms:

$$\dot{a} = \frac{3kb^3 \sin(\alpha - \beta)}{8\omega} - \frac{1}{2}\xi b \cos(\alpha - \beta) - \frac{f \sin\alpha}{2\omega}$$
(37)

$$a\dot{\alpha} = \frac{a\sigma}{2\omega} + \frac{3b^3 k \cos(\alpha - \beta)}{8\omega} + \frac{1}{2}b\xi \sin(\alpha - \beta)$$
$$- \frac{f \cos\alpha}{2\omega}$$
(38)

and

$$m\dot{a}\sin(\alpha - \beta) + ma\dot{\alpha}\cos(\alpha - \beta) + \frac{\xi}{2\omega}\dot{b} - mb\dot{\beta}$$

$$= -\frac{m\omega}{2}a\cos(\alpha - \beta) - \frac{3b^3 k}{8\omega} + \frac{m\omega}{2}b$$
(39)

$$m\dot{a}\cos(\alpha - \beta) - ma\dot{\alpha}\sin(\alpha - \beta) - m\dot{b} - \frac{\xi}{2\omega}b\dot{\beta}$$

$$= \frac{\xi}{2}b + \frac{m\omega}{2}a\sin(\alpha - \beta)$$
(40)

When the NES is disengaged, since the main system is linear, the amplitudes of the periodic solutions in x become

$$a_e = \frac{f}{\sigma}$$
(41)

$$\tan\alpha_e = \frac{a_e\sigma}{2\omega}$$
(42)

which are always stable. They are the equilibrium points of Eqs. (37), (38), when $b = 0$. Due to the lack of damping in the main system, the amplitude tends to infinite when σ goes to zero.

In the following analysis, the NES is considered engaged. The branches of equilibrium points of the dynamical system (37)–(40), which represent periodic oscillations in the original variables x and z, are shown in Fig. 4, for increasing values of f (in Fig. 4a when $f = 0.020$, in Fig. 4b when $f = 0.039$ and in Fig. 4c when $f = 0.075$). The figures are obtained via the software AUTO [22]. In the same figures, some equilibrium points are marked by colored points, to get reference with other subsequent figures, while black boxes represent Hopf bifurcation points. It can be observed that multiple solutions exist in some intervals of σ, as in Fig. 4a around $\sigma = -0.10$ or $\sigma = 0.10$. In Fig. 4b, around $\sigma = 0.2$, three solutions exist and

two of them are stable (green and yellow points, stable; red point, unstable); on the other hand, around the value $\sigma = -0.15$, three solutions exist and only one of them is stable (no colored points). A higher amplitude branch also exists, describing a closed island (only partially shown in the Figs. 4a, b). As the force is increased, the island gets wider and closer to the lower branch, until it disappears by merging with the lower branch (Fig. 4c). All these results are consistent with those shown in [2, 11].

Strongly modulated responses (SMR) are detected by numerical integration of the system (37)–(40). They represent quasiperiodic relaxation oscillations in the variables a and b, typically describing cycles around the two folds of the nonlinear manifold shown in Fig. 3. They are triggered in dependence of the position of the equilibrium points.

When $\sigma = 0.015$, $f = 0.02$, $m = 0.05$, $\xi = 0.01$, $\kappa = 0.067$, the equilibrium point is unique, unstable, and it is represented by the yellow point in Fig. 4a. In Fig. 5a, the same equilibrium point is shown (yellow point) on the nonlinear manifold (blue line), as well as the trajectory of the relaxation oscillation, describing an annular region (red line), while in Fig. 5b the latter is substituted by its Poincaré section (black points). The corresponding time evolutions of the amplitudes a, b (obtained by numerical integration of Eqs. (37)–(40)) and of the reconstituted displacements x, z are shown in Figs. 6a, b. They are in very good agreement with the solutions obtained by numerical integration of the original equations (31), (32), shown in Fig. 6c.

When $\sigma = 0.2$, $f = 0.039$, $m = 0.05$, $\xi = 0.01$, $\kappa = 0.067$, $\omega = 1$ (see Fig. 4b), the three different equilibrium points are marked with colored points. They are also shown in Fig. 7, lying on the nonlinear manifold. One of them is unstable (red point) and the other two are stable (green and yellow points). Two different trajectories are also shown Fig. 7 (magenta and black lines), asymptotically falling to the stable equilibria. Relaxation oscillations are not triggered and, therefore, periodic solution in x, z are obtained.

When $\sigma = -0.3$, $f = 0.075$, $m = 0.05$, $\xi = 0.01$, $\kappa = 0.067$, $\omega = 1$ (see Fig. 4c), the three different equilibrium points are marked and only the green one is stable. They are also shown in Fig. 8, on the nonlinear manifold. A relaxation oscillation is triggered, and its Poincaré section is shown (magenta points). For initial conditions close to the stable equilibrium point,
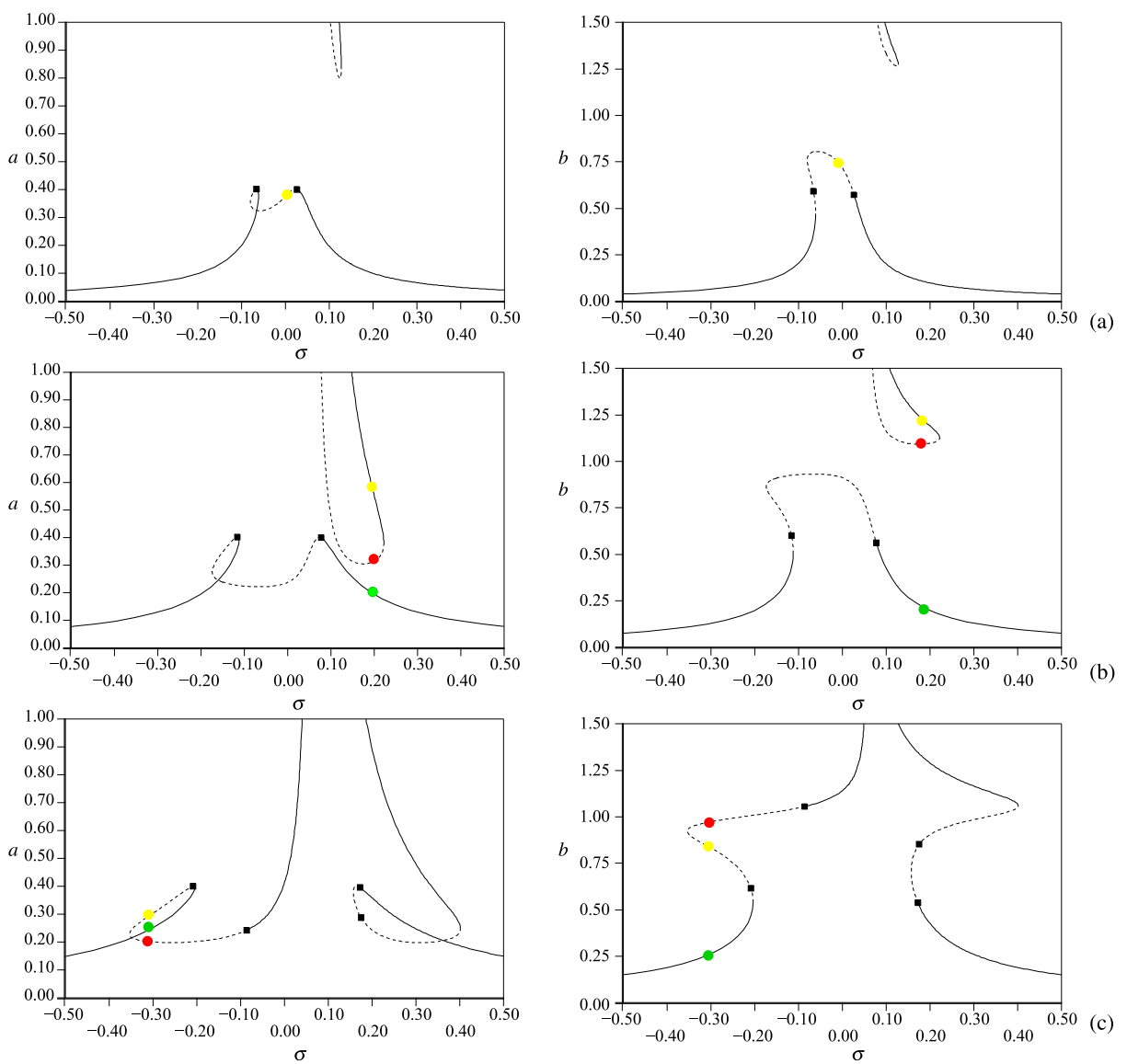
Fig. 4 Amplitudes a and b when NES is engaged, when $m = 0.05$, $\xi = 0.01$, $\kappa = 0.067$, $\omega = 1$, and (**a**) $f = 0.020$, (**b**) $f = 0.039$, (**c**) $f = 0.075$. The *filled squares* indicate Hopf bifurcation points. The colored points are equilibria referred to following figures. *Continuous line*: stable; *dashed line*: unstable

a trajectory asymptotically falling on it is also found (black line). The corresponding time evolutions of the amplitudes a, b and of the (reconstituted) displacements x, z are shown in Figs. 9a, b, in good agreement with the solutions obtained by numerical integration of the original equations (31), (32), shown in Fig. 9c.

In Fig. 10, the Poincaré map of the SMR is shown for smaller values of the NES parameters, $m = 0.005$, $\xi = 0.001$, $\kappa = 0.0067$, and for $\omega = 1$, $\sigma = -0.015$,

$f = 0.01$. The unique equilibrium point (yellow point) is stable and stands on the right branch of the nonlinear manifold. Also, trajectories falling to the equilibrium points are found, obtained when initial conditions close to the equilibrium point are considered. They are not reported in the figure. The SMR quasiperiodic time evolutions of a, b, and corresponding quasi-periodic time evolutions of x, z are shown in Figs. 11a, b, respectively. Again, they are in good agreement with the
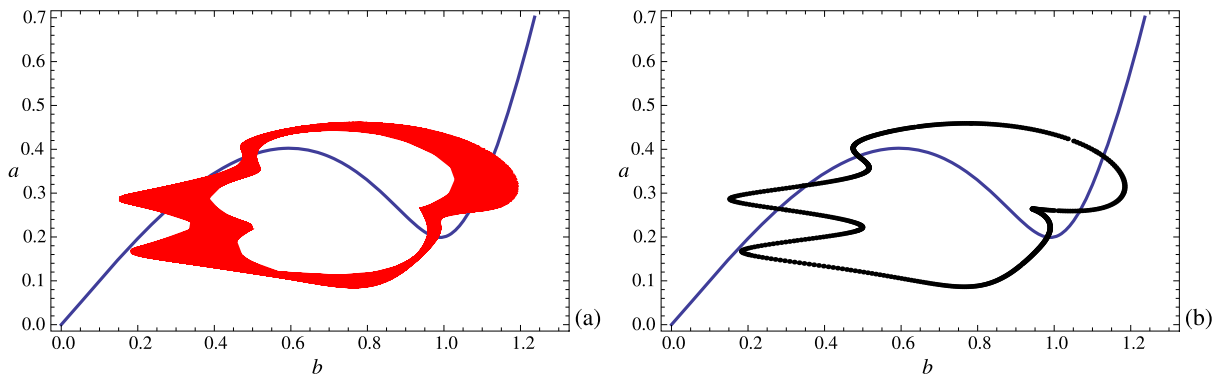
Fig. 5 Nonlinear manifold (*blue line*), equilibrium point (*yellow point*) and SMR: phase plot (**a**, *red line*) and Poincaré map (**b**, *black points*), when $\sigma = 0.015$, $f = 0.02$, $m = 0.05$, $\xi = 0.01$, $\kappa = 0.067$, $\omega = 1$
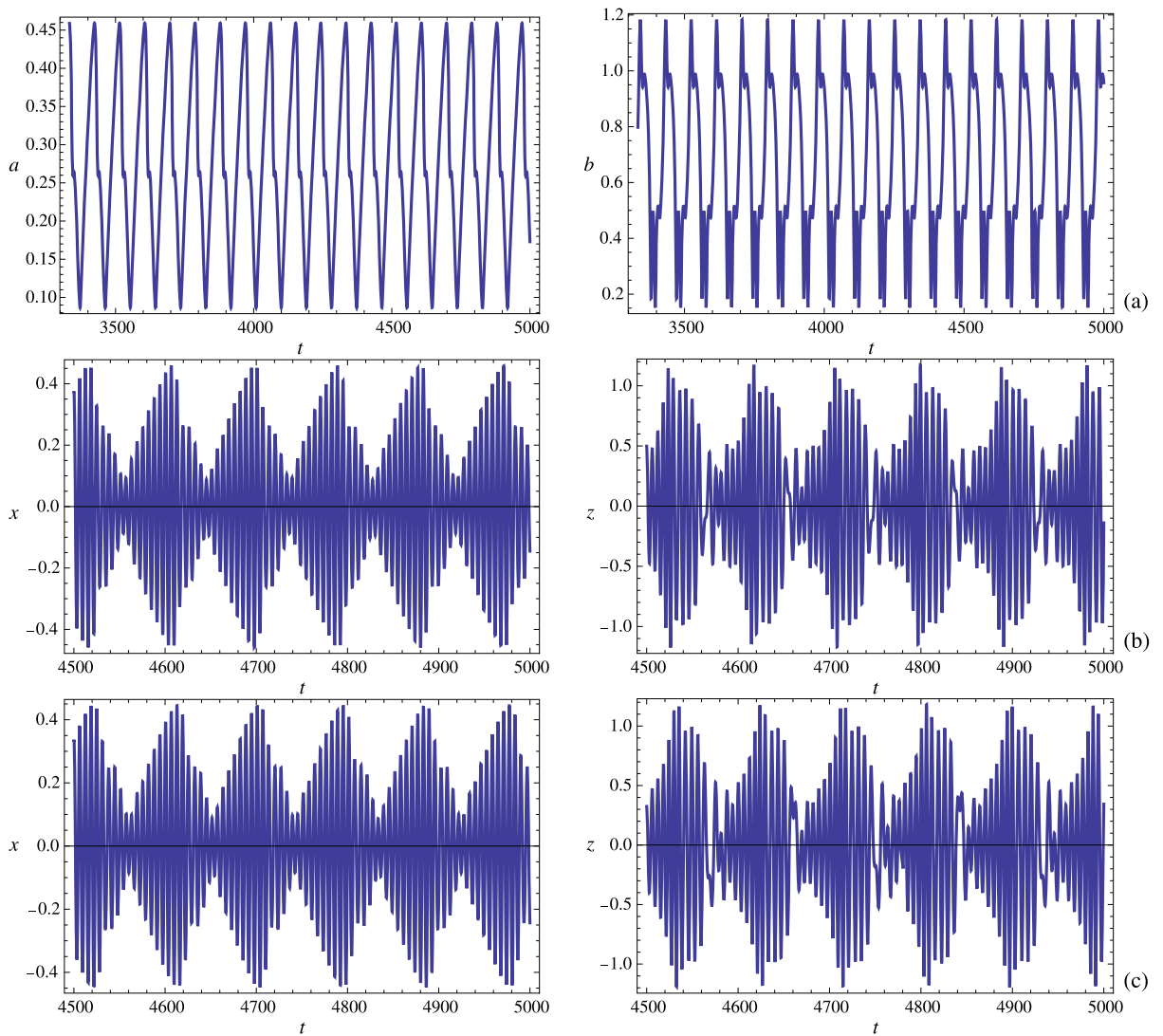

Fig. 6 SMR, when $\sigma = 0.015$, $f = 0.02$, $m = 0.05$, $\xi = 0.01$, $\kappa = 0.067$, $\omega = 1$; (**a**) amplitudes by MSHBM; (**b**) reconstituted response; (**c**) numerical integration of the original equations (31), (32)
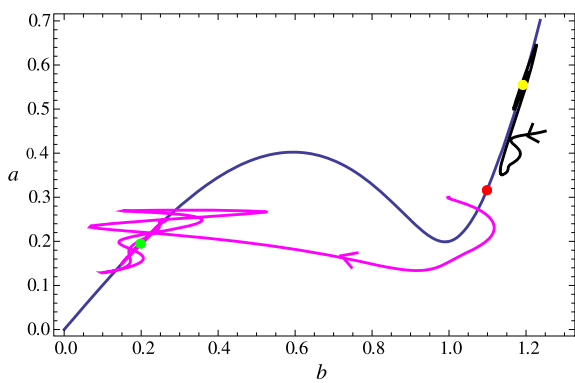
Fig. 7 Nonlinear manifold (*blue line*), three equilibrium points (*green*, *red*, and *yellow points*) and two transitional motions (*magenta* and *black lines*) falling to the equilibria, when $\sigma = 0.2$, $f = 0.039$, $m = 0.05$, $\xi = 0.01$, $\kappa = 0.067$, $\omega = 1$
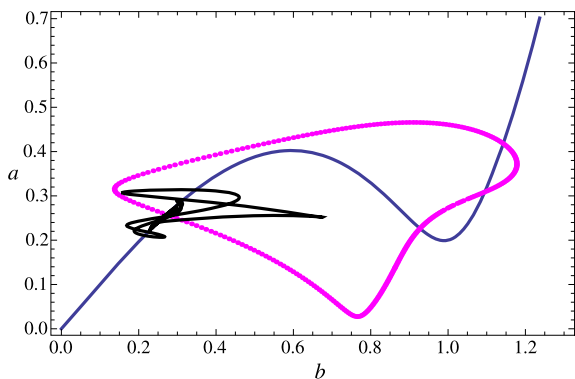

Fig. 8 Nonlinear manifold (*blue line*), three equilibrium points (*red*, *green* and *yellow points*), Poincaré map of the SMR response (*magenta points*), and transitional motion (*black line*) falling to the equilibrium point, when $\sigma = -0.3$, $f = 0.075$, $m = 0.05$, $\xi = 0.01$, $\kappa = 0.067$, $\omega = 1$

solution of the original equations (31), (32), shown in Fig. 11c.

4 Discussion

Few specific topics are now addressed, concerning the potentialities of the algorithm illustrated herein, namely, (a) the influence of higher harmonics, neglected in solving the NES equation, and (b) the analytical investigation of SMR, carried out in literature via a different approach.

4.1 Higher frequency-terms

The choice of using just one frequency-term, namely the one with frequency ω, in the Harmonic Balance

(i.e., in Eqs. (14), (21)), might appear as a strong limitation of the procedure introduced herein. In principle, indeed, terms of frequency $3\omega, 5\omega, \ldots$ could be involved and become significant.

To solve this issue, as a fist attempt, terms of frequency 3ω have been considered, also using

$$
z_0(t_0, t_1, \ldots)
$$
$$
= B_{11}(t_1, \ldots)e^{i\omega t_0} + B_{13}(t_1, \ldots)e^{3i\omega t_0} + cc
$$
$$
z_1(t_0, t_1, \ldots) \tag{43}
$$
$$
= B_{21}(t_1, \ldots)e^{i\omega t_0} + B_{23}(t_1, \ldots)e^{3i\omega t_0} + cc
$$

instead of Eqs. (14), (21), and obtaining corresponding equations which balance terms of frequency ω and 3ω, instead of Eqs. (15), (22), not reported here.

It turns out that the amplitudes of terms of frequency 3ω are always of higher order than those of frequency ω, and then resulting as negligible. They do not give any significant contribution to the dynamics of the system. In particular, after the reconstitution procedure ($B_1 := B_{11} + \varepsilon B_{21}$, $B_3 := B_{13} + \varepsilon B_{23}$, and coming back to the true time), if b_1 is the real amplitude of B_1 and b_3 is the real amplitude of B_3, the manifold should be naturally pictured as a curve in the three-dimensional space (b_1, b_3, a). For the numerical example considered in Sect. 3, it is shown in Fig. 12. The projection in the (b_1, a)-plane is practically the same of Fig. 3 whereas, looking at the projection in the (b_1, b_3)-plane, it can be observed that b_3 is much smaller than b_1 and a in the considered range. Corresponding results (not reported here) show that the effect of higher frequency 3ω is negligible in the equilibrium branches and SMR, also.

In any case, the presence of higher frequency-terms would preserve the structure of singular perturbation system, since Eqs. (24), (23) would be modified into:

$$
\dot{A} = f(A, \mathbf{B})
$$
$$
\varepsilon \dot{\mathbf{B}} = \mathbf{g}(A, \mathbf{B}) \tag{44}
$$

where $\mathbf{B} = \{B_1, B_3\}$.

4.2 Analytical detection of SMR

The analytical detection of the SMR can be accomplished with the outcomes of the MSHBM, as in the framework of the Manevitch complexification. This task is based on the study of the singularities of the
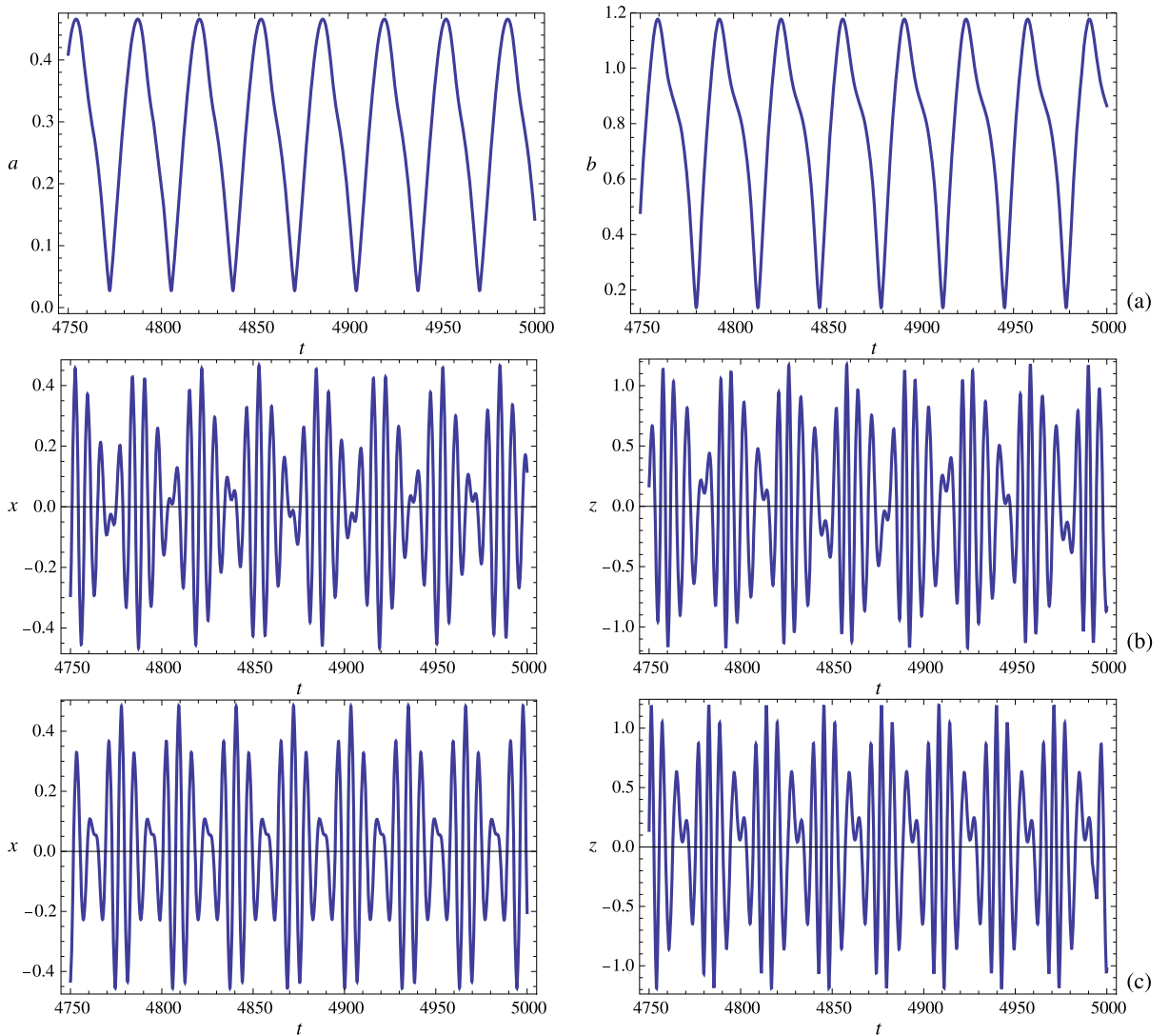
Fig. 9 SMR, when $\sigma = -0.3$, $f = 0.075$, $m = 0.05$, $\xi = 0.01$, $\kappa = 0.067$, $\omega = 1$; (**a**) amplitudes by MSHBM; (**b**) reconstituted response; (**c**) numerical integration of the original equations (31), (32)

slow dynamics on the manifold (see [11]). Already at the first perturbation step of the MSHBM, the slow dynamics on the manifold are addressed, whereas the second perturbation step allows the study of the dynamics also outside the manifold. In fact, if Eq. (15) is solved to obtain the expression

$$A = B_1 - \frac{i\xi B_1}{m\omega_1} - \frac{3k B_1^2 \bar{B}_1}{m\omega_1^2} \tag{45}$$

and it is substituted in Eq. (19), after coming back to the true time, the following complex differential equa-

tion in the dependent variables B_1, $\bar{B}_1$ is obtained:

$$\dot{B}_1 \left(-\frac{6k B_1 \bar{B}_1}{m\omega^2} - \frac{i\xi}{m\omega} + 1 \right) - \frac{3k B_1^2 \dot{\bar{B}}_1}{m\omega^2}$$

$$= \frac{if}{4\omega} + B_1^2 \bar{B}_1 \left(\frac{3ik\sigma}{2m\omega^3} - \frac{3ik}{2\omega} \right)$$

$$+ B_1 \left(-\frac{\xi\sigma}{2m\omega^2} + \frac{\xi}{2} - \frac{i\sigma}{2\omega} \right) \tag{46}$$

Using the polar representation $B_1(t) = \frac{1}{2}b(t)e^{i\beta(t)}$, and separating real and imaginary parts, two real dif-
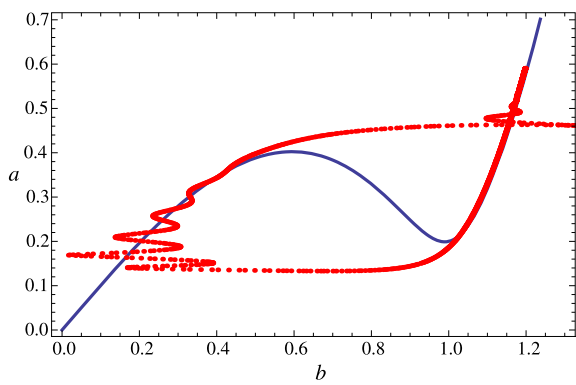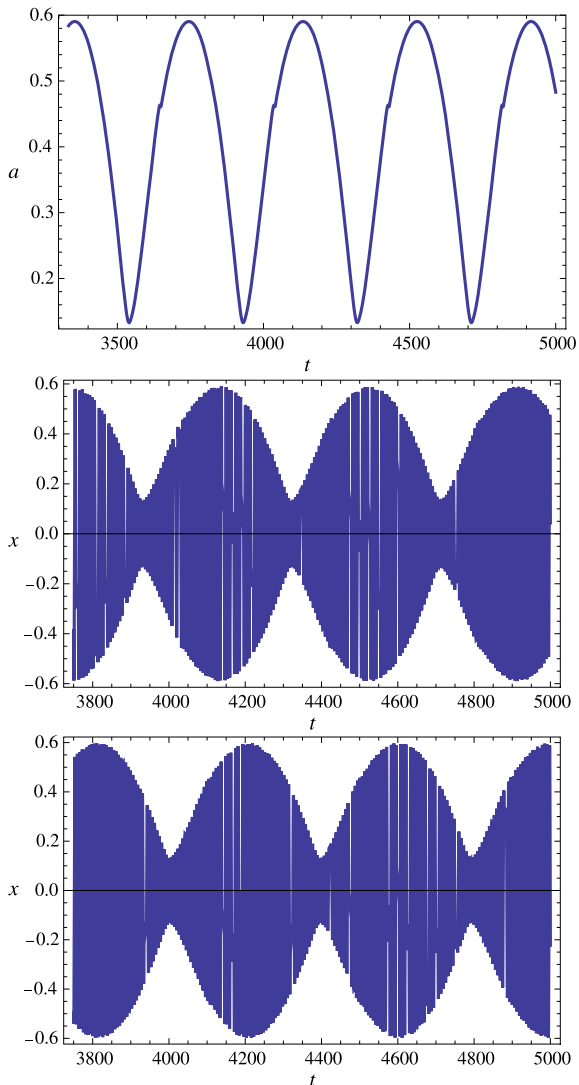
Fig. 10 Nonlinear manifold (*blue line*), equilibrium point (*yellow point*) and Poincaré map of the SMR response (*red points*), when $\sigma = -0.015$, $f = 0.01$, $m = 0.005$, $\xi = 0.001$, $\kappa = 0.0067$, $\omega = 1$

ferential equations in $b(t)$, $\beta(t)$ are obtained. The phase portrait in the stable sides of the manifold, representing $b(t)$ vs. $\beta(t)$, is shown in Fig. 13 for the numerical example, when $\sigma = 0.15$, $f = 0.02$, $m = 0.05$, $\xi = 0.01$, $\kappa = 0.067$, $\omega = 1$, where the limits of existence of the SMR, corresponding to the phases β_1 and β_2, are drawn by the vertical dashed lines.

5 Conclusions

In this paper, a general, nonlinear, multi-d.o.f. system, equipped with an essentially nonlinear oscillator with
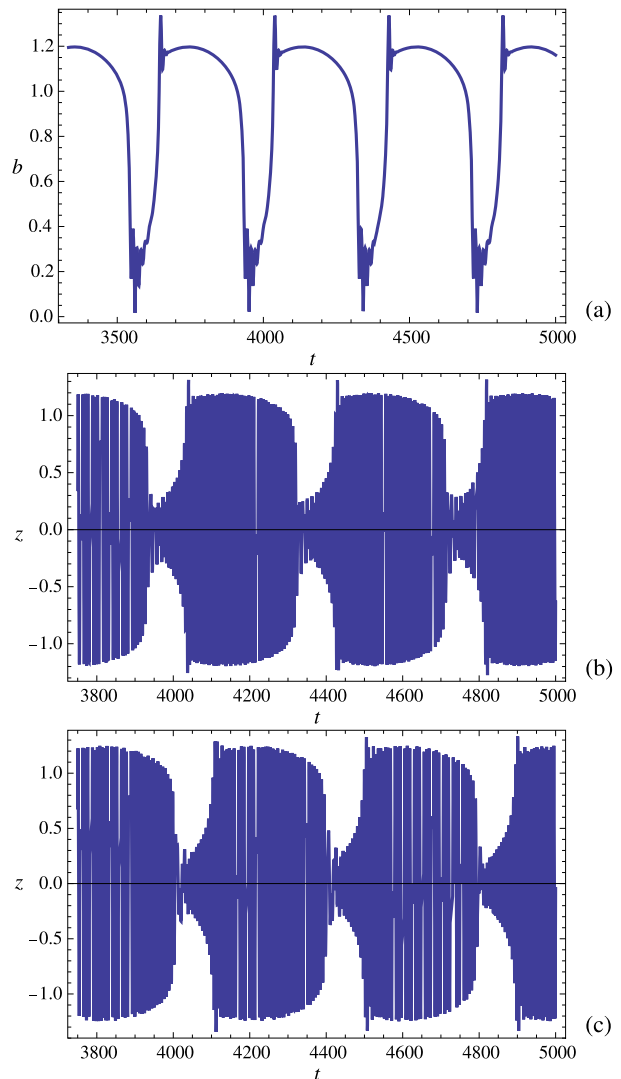

Fig. 11 SMR, when $\sigma = -0.015$, $f = 0.01$, $m = 0.005$, $\xi = 0.001$, $\kappa = 0.0067$, $\omega = 1$; (**a**) amplitudes by MSHBM; (**b**) reconstituted response; (**c**) numerical integration of the original equations (31), (32)
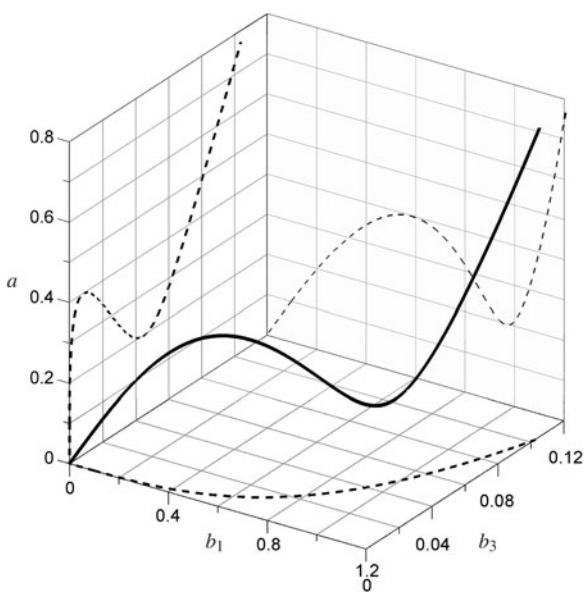
Fig. 12 Nonlinear manifold in (b_1, b_3, a)-space when both frequencies ω and 3ω are considered, when $\sigma = -0.3$, $f = 0.075$, $m = 0.05$, $\xi = 0.01$, $\kappa = 0.067$, $\omega = 1$
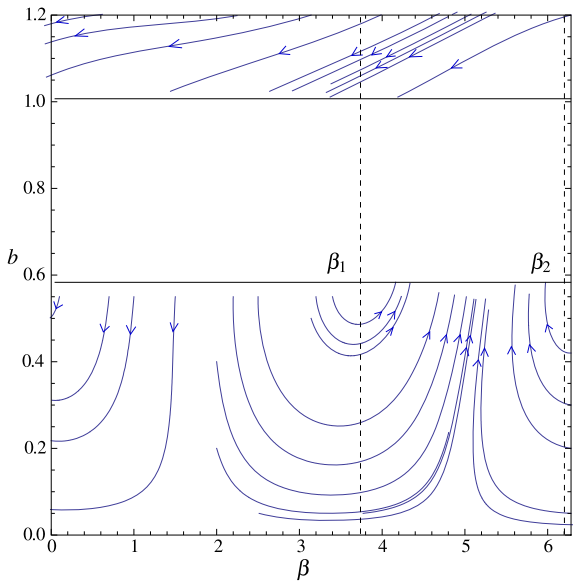

Fig. 13 Phase portrait of Eq. (46) in the stable sides of the manifold, when $\sigma = 0.15$, $f = 0.02$, $m = 0.05$, $\xi = 0.01$, $\kappa = 0.067$, $\omega = 1$

small mass (Nonlinear Energy Sink, NES), is considered. Aim of the NES is to passively control the amplitude of vibrations of the main system. A mixed Multiple Scale/Harmonic Balance Method (MSHBM) is proposed to get slow-flow dynamics, described by

singular perturbation equations. The main advantage of the procedure is that no complexification-averaging is required, so that the analysis is reconducted to the framework of the classical perturbation techniques. Numerical tests on a system, already analyzed in the literature, are pursued. The results show good agreement between the outcomes of the algorithm and direct integrations, in terms of equilibrium points and strongly modulation responses (SMR).

Appendix: Coefficients of the equations

The mode $\mathbf{u}$ is assumed normalized to get unitary modal mass ($\mathbf{u}^T \mathbf{M} \mathbf{u} = 1$). The expression of the coefficients of Eq. (19) are:

$$c_1 = -\frac{1}{2}\mathbf{u}^T\mathbf{C}\mathbf{u}, \qquad c_2 = -\frac{1}{2\omega}\mathbf{u}^T\mathbf{K}_1\mathbf{u}, \qquad c_3 = -\frac{\xi}{2}r$$

$$c_4 = \frac{3\kappa r}{2\omega}, \qquad c_5 = \frac{1}{2\omega}\mathbf{u}^T\mathbf{n}(\mathbf{u}, \mathbf{u}, \bar{\mathbf{u}}), \qquad c_6 = \frac{1}{4\omega}$$

$$(47)$$

In Eq. (20), the column matrices $\mathbf{w}_j$ ($j = 1, \ldots, 6$) are the solutions of the following singular algebraic problems in which, however, compatibility is satisfied:

$$\mathbf{w}_1: \quad (\mathbf{K}_0 - \omega^2\mathbf{M})\mathbf{w}_1 = -\omega(\mathbf{C}\mathbf{u} - (\mathbf{u}^T\mathbf{C}\mathbf{u})\mathbf{M}\mathbf{u}) \quad (48)$$

$$\mathbf{w}_2: \quad (\mathbf{K}_0 - \omega^2\mathbf{M})\mathbf{w}_2 = -(\mathbf{K}_1\mathbf{u} - (\mathbf{u}^T\mathbf{K}_1\mathbf{u})\mathbf{M}\mathbf{u}) \quad (49)$$

$$\mathbf{w}_3: \quad (\mathbf{K}_0 - \omega^2\mathbf{M})\mathbf{w}_3 = -\xi\omega(\mathbf{r} - r\mathbf{M}\mathbf{u}) \quad (50)$$

$$\mathbf{w}_4: \quad (\mathbf{K}_0 - \omega^2\mathbf{M})\mathbf{w}_4 = -3\kappa(\mathbf{r} - r\mathbf{M}\mathbf{u}) \quad (51)$$

$$\mathbf{w}_5: \quad (\mathbf{K}_0 - \omega^2\mathbf{M})\mathbf{w}_5$$
$$= -(\mathbf{n}(\mathbf{u}, \mathbf{u}, \bar{\mathbf{u}}) - (\mathbf{u}^T\mathbf{n}(\mathbf{u}, \mathbf{u}, \bar{\mathbf{u}}))\mathbf{M}\mathbf{u}) \quad (52)$$

$$\mathbf{w}_6: \quad (\mathbf{K}_0 - \omega^2\mathbf{M})\mathbf{w}_6 = -\frac{1}{2}(\mathbf{f} - f\mathbf{M}\mathbf{u}) \quad (53)$$

The solution is made unique by the normalization condition $\mathbf{w}_j^T \mathbf{u} = 0$.

Moreover, $\mathbf{w}_j$ ($j = 7, 8$) are the solutions of the following non-singular algebraic:

$$\mathbf{w}_7: \quad (\mathbf{K}_0 - 9\omega^2\mathbf{M})\mathbf{w}_7 = -\kappa\mathbf{r} \quad (54)$$

$$\mathbf{w}_8: \quad (\mathbf{K}_0 - 9\omega^2\mathbf{M})\mathbf{w}_8 = -\mathbf{n}(\mathbf{u}, \mathbf{u}, \mathbf{u}) \quad (55)$$

References

1. Vakakis, A.F., Gendelman, O.V., Bergman, L.A., McFarland, D.M., Kerschen, G., Lee, Y.S.: Nonlinear Targeted Energy Transfer in Mechanical and Structural Systems I. Springer, New York (2008a)
2. Vakakis, A.F., Gendelman, O.V., Bergman, L.A., McFarland, D.M., Kerschen, G., Lee, Y.S.: Nonlinear Targeted Energy Transfer in Mechanical and Structural Systems II. Springer, New York (2008b)
3. Maniadis, P., Kopidakis, G., Aubry, S.: Classical and quantum targeted energy transfer between nonlinear oscillators. Physica D **188**, 153–177 (2004)
4. Kerschen, G., Kowtko, J.J., McFarland, D.M., Bergman, L.A., Vakakis, A.F.: Theoretical and experimental study of multimodal targeted energy transfer in a system of coupled oscillators. Nonlinear Dyn. **47**, 285–309 (2007)
5. Panagopoulos, P.N., Gendelman, O., Vakakis, A.F.: Robustness of nonlinear targeted energy transfer in coupled oscillators to changes of initial conditions. Nonlinear Dyn. **47**, 377–387 (2007)
6. Aubry, S., Kopidakis, G., Morgante, A.M., Tsironis, G.P.: Analytic conditions for targeted energy transfer between nonlinear oscillators or discrete breathers. Physica B **296**, 222–236 (2001)
7. Tsakirtzis, S., Panagopoulos, P.N., Kerschen, G., Gendelman, O., Vakakis, A.F., Bergman, L.A.: Complex dynamics and targeted energy transfer in linear oscillators coupled to multi-degree-of-freedom essentially nonlinear attachments. Nonlinear Dyn. **48**, 285–318 (2007)
8. Guckenheimer, J., Hoffman, K., Weckesser, W.: Bifurcations of relaxation oscillations near folded saddles. Int. J. Bifurc. Chaos **15**, 3411–3421 (2005)
9. Guckenheimer, J., Wechselberger, M., Young, L.-S.: Chaotic attractors of relaxation oscillators. Nonlinearity **19**, 701–720 (2006)
10. Gendelman, O.V., Starosvetsky, Y., Feldman, M.: Attractors of harmonically forced linear oscillator with attached nonlinear energy sink i: description of response regimes. Nonlinear Dyn. **51**, 31–46 (2008)
11. Starosvetsky, Y., Gendelman, O.V.: Response regimes of linear oscillator coupled to nonlinear energy sink with harmonic forcing and frequency detuning. J. Sound Vib. **315**, 746–765 (2008)
12. Vaurigaud, B., Savadkoohi, A.T., Lamarque, C.-H.: Targeted energy transfer with parallel nonlinear energy sinks. Part I: design theory and numerical results. Nonlinear Dyn. **66**(4), 763–780 (2011a)
13. Savadkoohi, A.T., Vaurigaud, B., Lamarque, C.-H., Pernot, S.: Targeted energy transfer with parallel nonlinear energy sinks. Part II: theory and experiments. Nonlinear Dyn. **67**(1), 37–46 (2012)
14. Lamarque, C.-H., Gendelman, O.V., Savadkoohi, A.T., Etcheverria, E.: Targeted energy transfer in mechanical systems by means of non-smooth nonlinear energy sink. Acta Mech. **221**, 175–200 (2011)
15. Gendelman, O.V., Vakakis, A.F., Bergman, L.A., McFarland, D.M.: Asymptotic analysis of passive nonlinear suppression of aeroelastic instabilities of a rigid wing in subsonic flow. SIAM J. Appl. Math. **70**(5), 1655–1677 (2010)
16. Vaurigaud, B., Manevitch, L.I., Lamarque, C.-H.: Passive control of aeroelastic instability in a long span bridge model prone to coupled flutter using targeted energy transfer. J. Sound Vib. **330**, 2580–2595 (2011b)
17. Manevitch, L.: The description of localized normal modes in a chain of nonlinear coupled oscillators using complex variables. Nonlinear Dyn. **25**, 95–109 (2001)
18. Gendelman, O.V.: Targeted energy transfer in systems with non-polynomial nonlinearity. J. Sound Vib. **315**, 732–745 (2008)
19. Nayfeh, A.H., Mook, D.T.: Nonlinear Oscillations. Wiley, New York (1979)
20. Jiang, X., McFarland, D.M., Bergman, L.A., Vakakis, A.F.: Steady state passive nonlinear energy pumping in coupled oscillators: theoretical and experimental results. Nonlinear Dyn. **33**, 87–102 (2003)
21. Malatkar, P., Nayfeh, A.H.: Steady-state dynamics of a linear structure weakly coupled to an essentially nonlinear oscillator. Nonlinear Dyn. **47**, 167–179 (2007)
22. Doedel, E.J., Oldeman, B.E.: AUTO-07P: continuation and bifurcation software for ordinary differential equation (2012). URL http://cmvl.cs.concordia.ca/auto/